(2)

UNCLASSIFIED
SECURITY CLASSIFICATION OF THIS PAGE (When Data Entered)

REPORT DOCUMENTATION PAGE		READ INSTRUCTIONS BEFORE COMPLETING FORM
1. REPORT NUMBER: ARO 23928.6-GS	2. GOVT ACCESSION NO.: N/A	3. RECIPIENT'S CATALOG NUMBER: N/A
4. TITLE (and Subtitle): Multiple scattering corrections for lidar detection of obscured objects		5. TYPE OF REPORT & PERIOD COVERED: Applied Optics 29, 4170-4175 (1990)
		6. PERFORMING ORG. REPORT NUMBER
7. AUTHOR(s): T. Duracz and N.J. McCormick		8. CONTRACT OR GRANT NUMBER(s)
9. PERFORMING ORGANIZATION NAME AND ADDRESS: University of Washington, Seattle, WA 98195		10. PROGRAM ELEMENT, PROJECT, TASK AREA & WORK UNIT NUMBERS
11. CONTROLLING OFFICE NAME AND ADDRESS: U. S. Army Research Office, Post Office Box 12211, Research Triangle Park, NC 27709		12. REPORT DATE: 1 October 1990
		13. NUMBER OF PAGES: 6
14. MONITORING AGENCY NAME & ADDRESS (if different from Controlling Office)		15. SECURITY CLASS. (of this report): Unclassified
		15a. DECLASSIFICATION/DOWNGRADING SCHEDULE

16. DISTRIBUTION STATEMENT (of this Report)

Approved for public release; distribution unlimited.

17. DISTRIBUTION STATEMENT (of the abstract entered in Block 20, if different from Report)

NA

18. SUPPLEMENTARY NOTES

The view, opinions, and/or findings contained in this report are those of the author(s) and should not be construed as an official Department of the Army position, policy, or decision, unless so designated by other documentation.

19. KEY WORDS (Continue on reverse side if necessary and identify by block number)

Lidar, remote sensing, radiative transfer, obscuration

20. ABSTRACT (Continue on reverse side if necessary and identify by block number)

The importance of multiple scattering for lidar detection of a spherical object obscured by an aerosol is assessed using Monte Carlo radiative transfer calculations. Multiple scattering correction factors are significant and depend on the location and size of the object, and the field of view and time resolution of the detector.

DD FORM 1 JAN 73 1473 EDITION OF 1 NOV 65 IS OBSOLETE

UNCLASSIFIED
SECURITY CLASSIFICATION OF THIS PAGE (When Data Entered)

Multiple scattering corrections for lidar detection of obscured objects

T. Duracz and N. J. McCormick

The importance of multiple scattering for lidar detection of a spherical object obscured by an aerosol is assessed using Monte Carlo radiative transfer calculations. Multiple scattering correction factors are significant and depend on the location and size of the object, and the field of view and time resolution of the detector.

I. Introduction

Lidar detection and identification of objects is one of the important tasks in remote sensing. Since natural or man-made obscuring aerosols are often present, multiple scattering of the electromagnetic radiation can be a serious impediment to effective detection. Although the effect of multiple scattering when characterizing aerosols has been studied rather extensively,[1-7] its effect on lidar returns from objects is typically neglected by assuming a simple exponential attenuation along the optical path.

We consider the effect of multiple scattering on detection of a spherical object immersed in an obscuring aerosol, as schematically shown in Fig. 1. Both the source and detector are presumed to be at the same point (so the lidar is said to be monostatic). The incident lidar pulse at time $t = 0$ is located at $(x,y,z) = (0,0,0)$ and directed along the x-axis. The space bounded by planes $x = 0$ and $x = x_a$ is vacuum and the space between $x = x_a$ and $x = x_b$ is filled with aerosol. There is a diffusely reflecting plane boundary at $x = x_b$ with albedo a_b. For reasons of symmetry, a diffusely reflecting sphere of radius r_o and albedo a_o immersed in the aerosol can be taken to have its center (x_o,y_o,z_o) such that

$$x_a + r_o < x_o < x_b - r_o, \quad y_o \geq 0, \quad z_o = 0. \tag{1}$$

Within the detector field of view (FOV) consisting of a cone of half-angle θ measured in radians, all scatterings in the aerosol and reflections from objects can contribute to the time-resolved backscattered signal. The effect of multiple scattering increases with the FOV half-angle θ, which tends to make the object less discernible even though the total received signal is greater. The diameter d of the detector cone at the location of sphere, for example, is

$$d \approx 2\,\theta x_o, \tag{2}$$

and is greater than the diameter of the sphere when

$$\theta x_o > r_o. \tag{3}$$

To detect and identify the spherical object, the following are assumed known: distances x_a and x_b, albedo a_b, angle θ, and the single scatter albedo ω and the phase function $p(\mu)$ of the aerosol, where μ is the cosine of the angle between pre- and post-scattering directions; since the radiation is assumed to remain essentially monochromatic, the albedo and phase function do not depend upon wavelength. The phase function is normalized such that

$$2\pi \int_{-1}^{1} p(\mu)d\mu = 1. \tag{4}$$

The spatial variables x_o and y_o, the radius r_o, and albedo a_o of the spherical object are the four unknowns.

The nonanalog Monte Carlo method, which has been successfully applied in other remote sensing simulations,[1,2,4,6] has been chosen for the radiative transfer calculations because of the configuration of the 3-D geometry. In this method, a photon is tracked from one interaction in the aerosol or with the object to another by sampling for the distance to next interaction or escape from the aerosol, $\hat{r} = -\sigma^{-1} \ln\xi$, where σ is the aerosol attenuation coefficient in units of inverse length and ξ is a pseudorandom number on the interval $0 \leq \xi \leq 1$. At time t after the initial pulse, each photon carries a weight $w(t)$ that is proportional to the product of the nonabsorption probabilities of each preceeding collision. Whenever there is an interaction within the

The authors are with University of Washington, Department of Nuclear Engineering, Seattle, Washington 98195.

Received 4 December 1989.
0003-6935/90/284170-06$02.00/0.

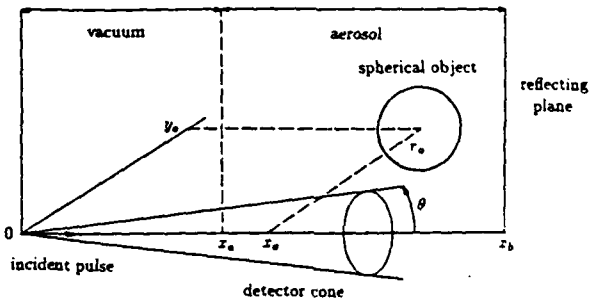

Fig. 1. Schematic of a spherical object embedded in an aerosol.

detection cone at time t_j, the ith photon causes a detector signal $S_{ij}(t)$ of

$$S_{ij}(t) = Kw(t_j)r^{-2}\exp(-d)p(\mu)\delta(t - t_j - r/v), \quad (5)$$

where r is the distance from the point of interaction to the detector, d is the corresponding optical distance to the detector, v is the speed of light, and K is a normalizing factor that is independent of time. The contributions to the signal from all scattering and reflections from the object or background surface are summed and placed in appropriate time bins to obtain the time-resolved simulated backscattered signal.

Before analyzing the effects of multiple scattering it is instructive to consider the case of an unobscured spherical object (or equivalently, one obscured by a nonabsorbing aerosol that is a perfect straight-ahead scatterer). If an instantaneous pulse is emitted at time $t = 0$ in the direction of the x-axis and the spherical object is centered at $(x_o,y_o,0)$, the total returned signal received by the detector is given by

$$S(t) = K(a_o/2\pi)r^{-2}\delta(t - 2r/v), \quad y_o < r_o,$$
$$= 0, \quad \text{otherwise.} \quad (6)$$

This result follows from Eq. (5) with $d = 0$ and $w = 1$, since there is only a single reflection from the object and no attenuation along the path, and since $p(\mu) = a_o/2\pi$ corresponding to an equal probability for scattering in any direction leaving the surface. From the time delay $t_d = 2r/v$ after the initial pulse and the magnitude of the time-integrated return $S_o = Kr^{-2}a_o/2\pi$ in Eq. (6) it is possible to estimate the distance to the sphere and its albedo,

$$r = t_d v/2, \quad (7)$$

$$a_o = S_o\pi(t_d v)^2/2K. \quad (8)$$

The location (x_o,y_o) of the object and its radius r_o are linked to the distance r through

$$(x_o - r)^2 + y_o^2 = r_o^2. \quad (9)$$

It is worth noting that the localized return in time in Eq. (6) depends on a localized spot illumination. With a larger area of illumination, however, there can be considerable geometric pulse broadening.[8]

When an aerosol is present, Eq. (6) must be modified to account for the possibility of backscattering from either the aerosol or the object. If the aerosol is optically thin enough or the detector FOV angle θ is small enough, only once-scattered photons need be considered. The returned signal $S^{(1)}(t)$ received by the detector is then

$$S^{(1)}(t) = K\exp[-2d(t/2)]|2(vt)^{-2}\omega p(-1)$$
$$\times [\Theta(t - 2x_a/v) - \Theta(t - 2r/v)]$$
$$+ r^{-2}(a_o/2\pi)\delta(t - 2r/v)\}, \quad y_o < r_o,$$
$$= K\exp[-2d(t/2)]2(vt)^{-2}\omega p(-1)\Theta(t - 2x_a/v), \quad y_o > r_o, \quad (10)$$

where $d(t) = \sigma(vt - x_a)$ is the optical distance from an interaction point to the detector, r is the distance from the object to the detector, and $\Theta(t)$ is the step function:

$$\Theta(t) = 1, \quad t \geq 0,$$
$$= 0, \quad t < 0. \quad (11)$$

When the aerosol is so thick that multiple scatterings must be taken into account, the total signal received by the detector from all the photons is

$$S(t) = \sum_{ij} S_{ij}(t) = B(t) + R(t), \quad (12)$$

which is the sum of the backscattered signal $B(t)$ generated by one or more scatterings in the aerosol and the reflected signal $R(t)$ from at least one reflection from the object, with possibly one or more scatterings before or after reflection. In a sense, $B(t)$ represents pure noise since there is no information about the object.

The signal obtained in an actual measurement is always averaged over a small interval of time. Likewise, in the Monte Carlo method this occurs when the detector count rate is tallied in the kth time bin Δt_k. In practice this means that $S(t)$ in Eq. (12) is of the form

$$S_k = \sum_{ij}\int_{\Delta t_k} S_{ij}(t)dt, \quad (13)$$

where the time interval Δt_k is defined such that

$$\Delta t_k = [(k - 1)\Delta t, k\Delta t], \quad k \geq 1. \quad (14)$$

Multiple scattering can be expressed in the form of a multiple scattering correction,

$$C_k = S_k\left[N\int_{\Delta t_k} S^{(1)}(t)dt\right]^{-1}, \quad (15)$$

which is the ratio of the total return to the single scattering return from Eq. (10), with N the number of photons used in the simulation. The multiply-scattered returned signal $S(t) - S^{(1)}(t)$ is noncoherent due to the random nature of the scatterings in the aerosol. Thus this portion of the returned signal would contribute directly to the total signal measured by a noncoherent lidar detector, as assumed in this paper, or would contribute to the background noise of a coherent (heterodyne) lidar detector.

II. Procedure for Numerical Tests

The phase function $p_G(\mu)$ of the obscuring aerosol was obtained from a Mie scattering calculation for

spherical particulates with size parameter $\alpha = 2\pi a/\lambda$, where a is the sphere radius and λ is the radiation wavelength. A Gaussian distribution of sizes was assumed[8] with a mean value of $\langle\alpha\rangle = 10$ and a standard deviation of $\sigma = 2$. A nonabsorbing medium ($\omega = 1$) with a refractive index of $n - ik = 1.3$ was selected, and this resulted in a moderately forward oriented scattering.[8]

The unit of length for the calculations was taken to be the mean free path between scatterings in the aerosol, and the unit of time was the mean time between scatterings, so that $v = 1$. The distance from the lidar to the edge of the aerosol was arbitrarily set to $x_a = 3$; this distance translates the time axis of all calculations and also influences the geometry of the problem.

An important parameter in the study was the time resolution of the detector, i.e., the duration of each time bin Δt. The values varied from 0.05 to 0.25.

To maximize the lidar return, a nonabsorbing sphere ($a_o = 1$) was placed on the x-axis ($y_o = 0$). Two values of the sphere radius were selected, $r_o = 0.01$ and 0.1, while the background plane boundary was placed far away from the sphere ($x_b = \infty$). The values of x_o and θ remained variable, in addition to Δt, so $S_k = S_k(x_o,\theta,\Delta t)$ and $C_k = C_k(x_o,\theta,\Delta t)$.

An estimate of the relative error e_k associated with

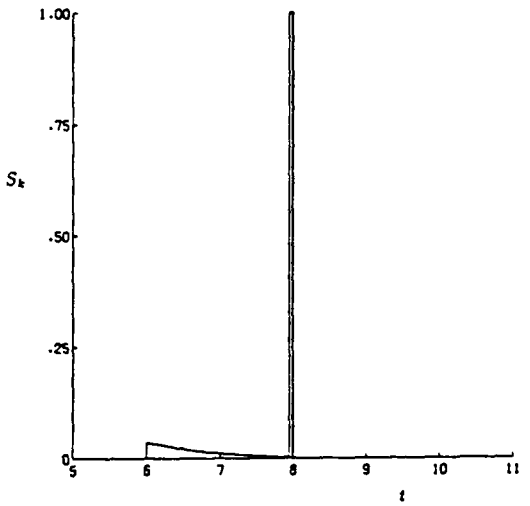

Fig. 2. Returned signal vs time for a sphere of radius 0.01 with its center at distance 4 from a lidar whose FOV half-angle is 5×10^{-3} rad. Time bin duration is 0.05.

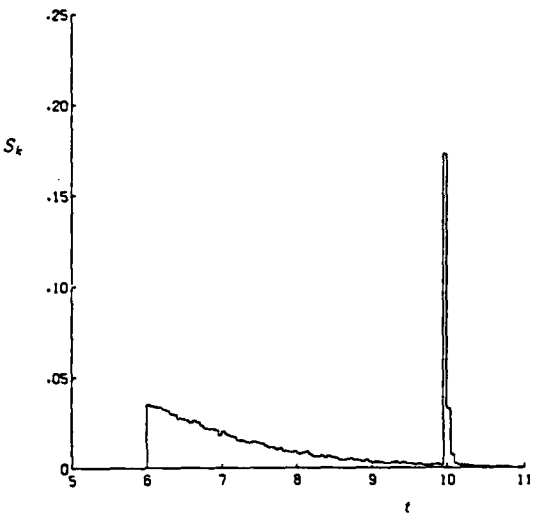

Fig. 4. Returned signal normalized to that in Fig. 2 vs time for a sphere of radius 0.01 with its center at distance 5 from a lidar whose FOV half-angle is 5×10^{-2} rad. Time bin duration is 0.05.

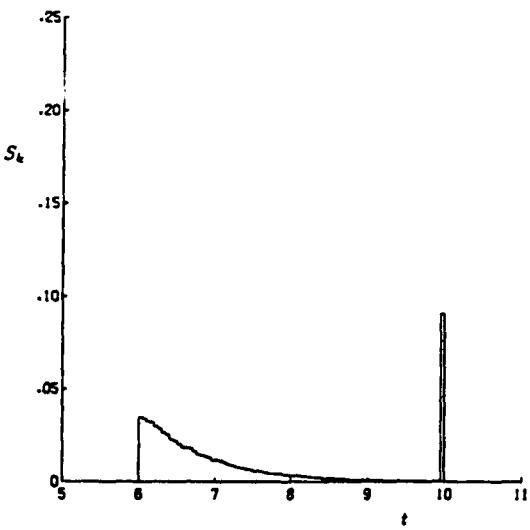

Fig. 3. Returned signal normalized to that in Fig. 2 vs time for a sphere of radius 0.01 with its center at distance 5 from a lidar whose FOV half-angle is 5×10^{-3} rad. Time bin duration is 0.05.

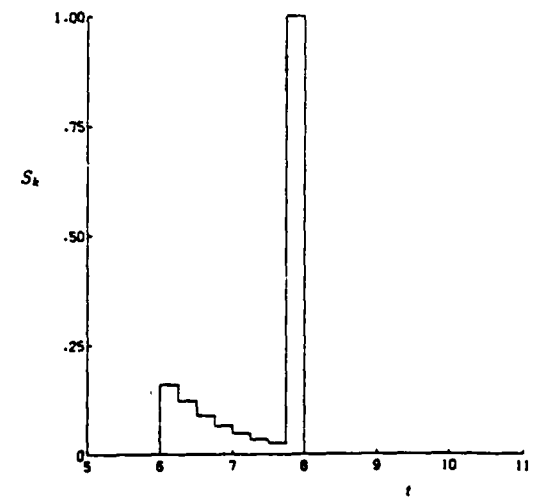

Fig. 5. Returned signal vs time for a sphere of radius 0.01 with its center at distance 4 from a lidar whose FOV half-angle is 5×10^{-3} rad. Time bin duration is 0.25.

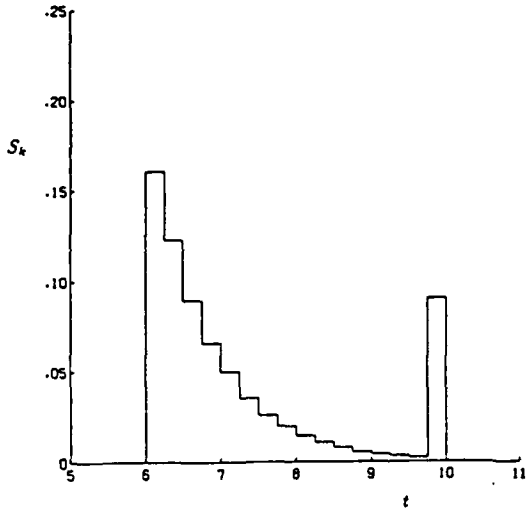

Fig. 6. Returned signal normalized to that in Fig. 5 vs time for a sphere of radius 0.01 with its center at distance 5 from a lidar whose FOV half-angle is 5×10^{-3} rad. Time bin duration is 0.25.

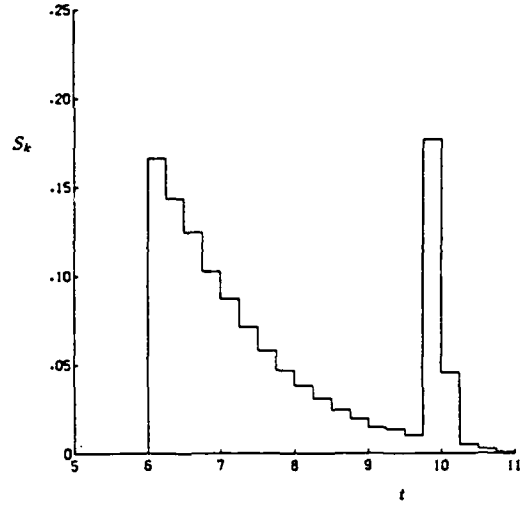

Fig. 7. Returned signal normalized to that in Fig. 5 vs time for a sphere of radius 0.01 with its center at distance 5 from a lidar whose FOV half-angle is 5×10^{-2} rad. Time bin duration is 0.25.

S_k for N photon histories can be obtained from

$$e_k = S_k^{-1}\left\{\sum_{ij}\left[\int_{\Delta t_k} S_{ij}(t)dt\right]^2\right\}^{1/2}. \quad (16)$$

For large N this becomes identical with the estimated standard deviation of the mean tallied signal divided by the mean signal. The computer simulations were made with $N = 5 \times 10^5$ or 10^6, and the value of e_k did not exceed a few percent even for cases with the smallest time bins $\Delta t = 0.05$.

III. Effect of Multiple Scattering

Examples of the simulated signal return S_k obtained as in Eq. (13) are shown in Figs. 2–4 for a sphere of radius $r_o = 0.01$ and time bins of duration $\Delta = 0.05$. The values are normalized to the maximum value of unity in Fig. 2.

In Fig. 2 the distance to the lidar is $x_o = 4$ and the detector FOV half-angle is $\theta = 5 \times 10^{-3}$ rad, while in Fig. 3 the distance to the lidar has been increased to $x_o = 5$ with the same FOV. The strong damping effect of the additional intervening aerosol is visible. In Fig. 4 the distance is $x_o = 5$, as in Fig. 3, but the FOV has been increased to $\theta = 5 \times 10^{-2}$ rad. The received signal is stronger because of additional radiation scattered from the object and aerosol and a slight spreading in time of the signal also occurs.

In Figs. 5–7 all the parameters are identical to those in Figs. 2–4 except that $\Delta t = 0.25$ instead of 0.05. As Δt increases the peak value of the returned signal appears smaller relative to the returned signal in other bins because of the aerosol. Also, by comparing Figs. 4 and 7 an apparent broadening of the returned signal near the peak can be seen for the case with larger Δt. This broadening is sensitive to the precise location of the Δt_k relative to twice the transit time between the lidar and the object, $2(x_o - r_o)$, since it may happen that part of the contribution of the returned signal from the object gets recorded in adjacent time bins.

Because the peak value of the returned signal is of principal interest, we now focus on the correction factor $C_{sp}(x,\theta,\Delta t)$, the $C_k(x_o,\theta,\Delta t)$ in Eq. (15) for a time bin Δt_{sp} symmetrically located about the time of the peak signal return:

$$\Delta t_{sp} = [2(x_o - r_o) - \Delta t/2,\ 2(x_o - r_o) + \Delta t/2]. \quad (17)$$

$C_{sp} = 1$ in the limiting case of no aerosol ($x_o = x_a$) and when multiple scattering is insignificant ($\theta \to 0$ or $\Delta t \to 0$). For the values of our example calculations, the principal changes in C_{sp} occur for $x_a \le x_o \le x_a + 2$ (where $x_a = 3$) and $10^{-3} \le \theta \le 10^{-1}$ rad.

The results for C_{sp} with a spherical object of radius $r_o = 0.01$ and $\Delta t = 0.05$, 0.15, and 0.25 are shown in Figs. 8–10. (Note the different scales for the C_{sp} values.) The multiple scattering correction increases to signifi-

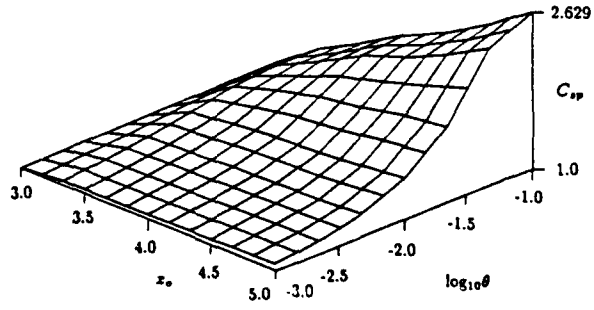

Fig. 8. Multiple scattering correction factor for the symmetric peak time bin for a sphere of radius 0.01 vs the lidar-to-sphere center distance and detector FOV half-angle. Symmetric time bin duration is 0.05.

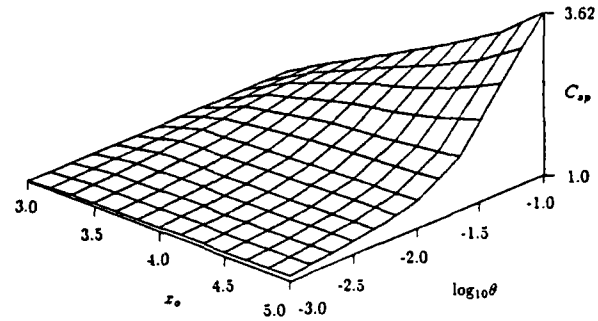

Fig. 9. Multiple scattering correction factor for the symmetric peak time bin for a sphere of radius 0.01 vs the lidar-to-sphere center distance and detector FOV half-angle. Symmetric time bin duration is 0.15.

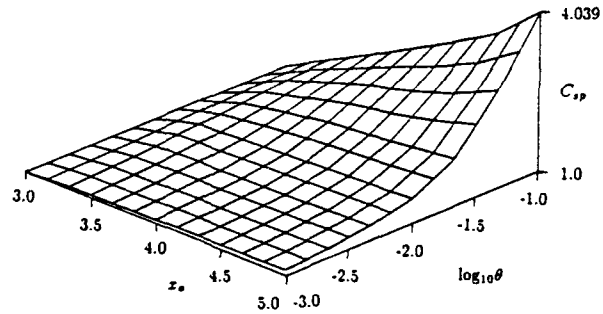

Fig. 10. Multiple scattering correction factor for the symmetric peak time bin for a sphere of radius 0.01 vs the lidar-to-sphere center distance and detector FOV half-angle. Symmetric time bin duration is 0.25.

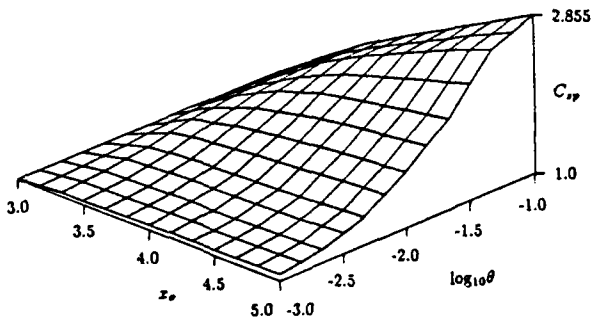

Fig. 11. Multiple scattering correction factor for the symmetric peak time bin for a sphere of radius 0.1 vs the lidar-to-sphere center distance and detector FOV half-angle. Symmetric time bin duration is 0.05.

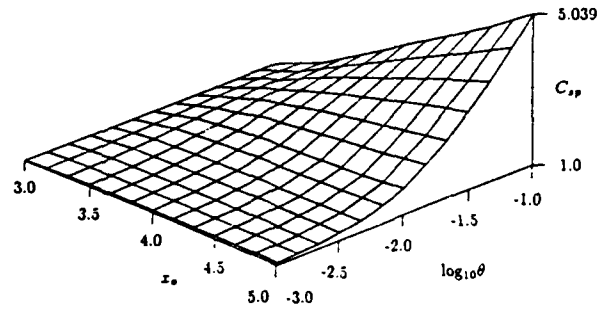

Fig. 12. Multiple scattering correction factor for the symmetric peak time bin for a sphere of radius 0.1 vs the lidar-to-sphere center distance and detector FOV half-angle. Symmetric time bin duration is 0.25.

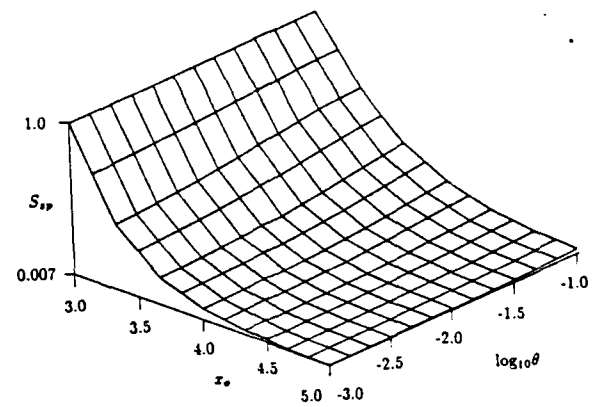

Fig. 13. Normalized returned signal for a sphere of radius 0.01 vs the lidar-to-sphere center distance and detector FOV half-angle. Symmetric time bin duration is 0.25.

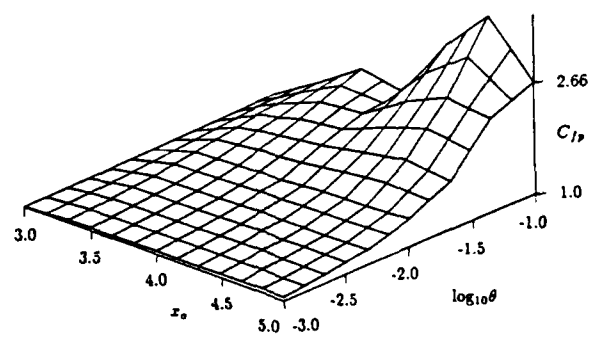

Fig. 14. Multiple scattering correction factor for a fixed time bin grid for a sphere of radius 0.01 vs the lidar-to-sphere center distance and detector FOV half-angle. Time bin duration is 0.25.

cant values for larger distances x_o and larger FOV half-angles θ. The effect is even more pronounced for a sphere of radius $r_o = 0.1$, as seen in Figs. 11 and 12 for $\Delta t = 0.05$ and 0.25, respectively.

The rising values of C_{sp} also reflect the fact that the returned signal decreases rapidly as the lidar-to-sphere distance increases. Figure 13 shows the decrease in S_{sp}, the normalized returned signal in bin Δt_{sp}, for $r_o = 0.01$ and $\Delta t = 0.25$. A very similar pattern occurs for any other of the assumed r_o and Δt values.

If the multiple scattering correction factor is calculated using a fixed time bin grid, as in Eq. (14), the peak return signal $S(t)$ will sometimes occur near the beginning or end of a time bin, as mentioned earlier, and a fraction of the time-broadened peak return will be

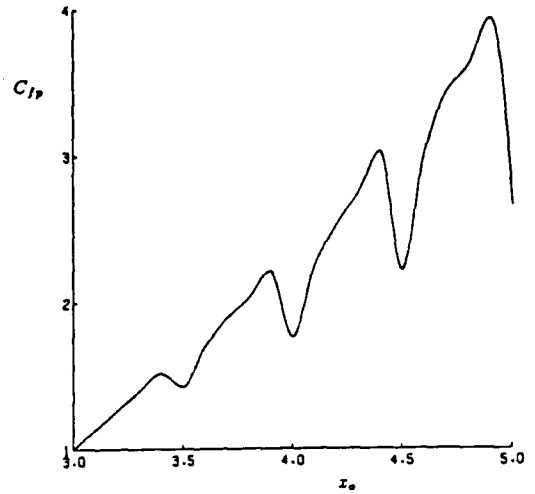

Fig. 15. Multiple scattering correction factor for a fixed time bin grid for a sphere of radius 0.01 vs the lidar-to-sphere center distance. The detector FOV half-angle is 10^{-1} and the time bin duration is 0.25 rad.

counted in an adjacent bin. Figure 14 illustrates the correction factor C_{fp} for such a case of a fixed time bin grid with $\Delta t = 0.25$ and $r_o = 0.01$; C_{fp} is the same as C_k of Eq. (15) for the time bin k in which the peak occurs. The figure should be compared with Fig. 10 for C_{sp} that was calculated for the symmetric time bin in Eq. (17). There is a clear periodic pattern in Fig. 14 that appears even more dramatic in the enhanced view in Fig. 15 for the case of the large FOV half-angle of $\theta = 10^{-1}$ rad. The spacing of the pattern corresponds to $2\Delta t$, the additional transit time for the signal if the sphere is near the end of the time bin in the fixed grid instead of at the beginning.

IV. Conclusions

Monte Carlo calculations have been performed to assess the effect of multiple scattering on a lidar return signal from a spherical object obscured by an aerosol. Figures 2–7 demonstrate the expected sharp peak in the returned signal caused by the presence of the object, with some signal decrease and broadening for larger distances and detector FOVs. The importance of multiple scattering is illustrated in Figs. 8-12 for a time bin symmetrically located about the peak value of the time-dependent return signal. We found that it is important to distinguish between the use of a symmetric time bin located about the peak signal return (as in Fig. 10) and a fixed bin location (as in Fig. 14) in calculating the multiple scattering correction factor.

This work was supported by U.S. Army Research Office contract DAAL03-86-K-0118 and by the San Diego Supercomputer Center.

References

1. G. N. Plass and G. W. Kattawar, "Monte Carlo Calculations of Light Scattering from Clouds," Appl. Opt. 7, 415–419 (1968).
2. G. N. Plass and G. W. Kattawar, "Reflection of Light Pulses from Clouds," Appl. Opt. 10, 2304–2310 (1971).
3. R. C. Anderson and E. V. Browell, "First- and Second-Order Backscattering from Clouds Illuminated by Finite Beams," Appl. Opt. 11, 1345–1351 (1972).
4. K. E. Kunkel and J. A. Weinman, "Monte Carlo Analysis of Multiply Scattered Lidar Returns," J. Atmos. Sci. 33, 1772–1781 (1976).
5. I. V. Samokhvalov, "Double-Scattering Approximation of Lidar Equation for Inhomogeneous Atmosphere," Opt. Lett. 4, 12–14 (1978).
6. C. M. R. Platt, "Remote Sounding of High Clouds. III: Monte Carlo Calculations of Multiple-Scattered Lidar Returns," J. Atmos. Sci. 38, 156–167 (1981).
7. W. G. Tam, "Aerosol Backscattering of a Laser Beam," Appl. Opt. 22, 2965–2969 (1983).
8. T. Duracz and N. J. McCormick, "Radiative Transfer Calculations for Characterizing Obscured Surfaces Using Time-Dependent Backscattered Pulses," Appl. Opt. 28, 544–552 (1989).